Corrosion inhibition effect of 1-butyl-3-methyl-1H-benzimidazolium iodide for 2205 duplex stainless steel in hydrochloric acid solution

Xiong Zhang[1,3], Jiewen Li[2], Xingwen Zheng[2, 3,*], Min Gong[1,3], Wilfred Emori[3], Wenpo Li[4], Bochuan Tan[4]

[1] School of Chemical Engineering, Sichuan University of Science & Engineering, Zigong 643000, China
[2] School of Chemistry and Environmental Engineering, Sichuan University of Science & Engineering, Zigong 643000, China
[3] Key Laboratory of Material Corrosion and Protection of Sichuan Province, Zigong 643000, China
[4] School of Chemistry and Chemical Engineering, Chongqing University, Chongqing 400044, China
[*]E-mail: zxwasd@126.com

The anticorrosion properties of 1-butyl-3-methyl-1H-benzimidazolium iodide (BMBM) for 2205 duplex stainless steel in 1.0 M HCl solution has been evaluated by electrochemical techniques (potentiodynamic polarization and electrochemical impedance spectroscopy) and scanning electron microscopy. The effect of temperature and concentration on the inhibition efficiency have also been studied. The results reveal that BMBM is a mixed-type inhibitor whose adsorption obeys the Langmuir adsorption isotherm. The inhibition efficiency increased with increase in concentration, but decreased when the temperature was raised. The results obtained from kinetic analysis were compared with those of electrochemical techniques and they confirmed that BMBM is an effective green corrosion inhibitor for 2205 duplex stainless steel in 1.0 M HCl.

Keywords: 2205 duplex stainless steel, Hydrochloric acid, Corrosion inhibitor, Adsorption isotherm, Kinetic analysis

1. INTRODUCTION

Duplex stainless steel is widely used in various fields of modern industrial society because of its good corrosion and oxidation resistance [1, 2]. 2205 duplex stainless steel (2205 DSS) which comprises of an approximately equal amount of ferrite and austenite with high amounts of other key elements has a higher corrosion resistance than the conventional stainless steel [3-11]. However, it is still prone to corrosion in some industrial processes, such as oil well acidizing, acid cleaning, and acid descaling [12,

13]. An efficient approach to prevent the corrosion of equipment made of stainless steel is the use of corrosion inhibitors. For example, Kurniawan and Madurani [14] studied red pepper seed oil as a corrosion inhibitor for 304 stainless steel (304 SS) in 1.0 M HCl solution, and they reported the formation of thin layers on the 304 SS surface that blocked the metal-aggressive solution interactions. Matos et al [15] showed that barley agro-industrial waste was a corrosion inhibitor for stainless steel AISI 304 in H_2SO_4. They found that it exhibited inhibition efficiency up to 97% and was physically adsorbed on the metal surface. Soltani [16], using weight loss method and electrochemical measurements, showed that silybum marianum leaves extract behaved as mixed-type inhibitor, and the adsorption of the extract constituents obeyed Langmuir adsorption isotherm.

Ionic liquids, which are molten salts composed of organic cations and various anions, are seen as emerging and reliable substitutions for conventional corrosion inhibitors. They have the advantage of being designed into different cations/anions in addition to being able to vary the type and position of substituent. Most importantly, these solvents have numerous excellent properties, such as low melting point, non-flammability, high ionic conductivity, excellent thermal stability, and relatively low volatility over normal operating temperature range [17-19]. Ionic liquids have been employed in corrosion inhibition studies for steel in various solutions. For example, Shetty et al [20] evaluated the properties of an ionic liquid corrosion inhibition on 6061 Al-15 vol. pct. SiC (P) composite in 0.1 M HCl and 0.1 M H_2SO_4. Inhibition efficiencies of 98.7% in HCl and 98.8% in H_2SO_4 were achieved, and it acted as a mixed-type inhibitor with predominant cathodic control. Zheng et al [21] reported that the El-Awady thermodynamic–kinetic model was obeyed with good inhibition performances when they studied the effect of 1-octyl-3-methylimidazolium bromide and 1-allyl-3-octylimidazolium bromide on mild steel in 0.5 M H_2SO_4. Also, Kannan et al [22] proposed a mechanism of corrosion inhibition from the results of electrochemical methods of mild steel after immersion in 1.0 M HCl containing synthesized 3-(4-chlorobenzoylmethyl)-1-methylbenzimidazoliumbromide. They also reported that the ionic liquid was a good inhibitor that functioned by adsorption and obeyed the Langmuir adsorption isotherm. Our previous study was on the critical pitting temperature of 2205 DSS in different concentrations of NaCl solution [23], whereas we are investigating the protection of the metal in a typical acid environment in the current study.

Presently, to the best of our knowledge, there is no report on the inhibitive effects of BMBM (see chemical structure in Figure 1) on acid corrosion of 2205 DSS in 1.0 M HCl solution. Therefore, it became necessary to conduct a detailed investigation on the effect of BMBM, an ionic liquid, on the acid corrosion of 2205 DSS in 1.0 M HCl solution. Potentiodynamic polarization and electrochemical impedance spectroscopy (EIS) experiments were used in the present work to assess the inhibition efficiency of the ionic liquid while scanning election microscopy was utilized to confirm the presence of adsorbed film layers on the surface of 2205 DSS. The effect of temperature on the corrosion reaction rate was also investigated and discussed.
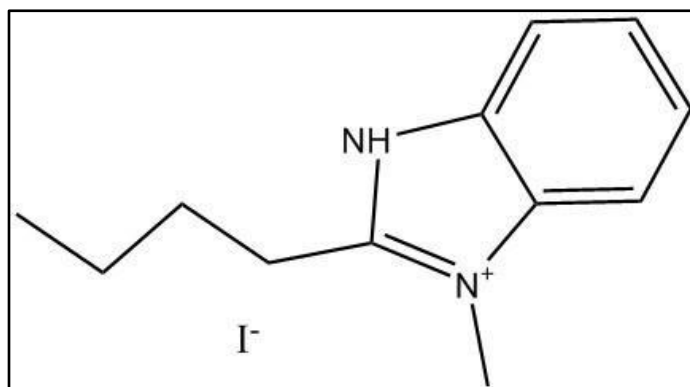
Figure 1. The chemical structure of BMBM.

2. EXPERIMENTAL

2.1 Material and electrolyte

2205 DSS was used as the working electrode for the experiment. Its composition (in weight percentage) is listed in Table 1. The received metal was a round rod with 16.0 mm diameter. The test coupons which were cut out from the metal for surface analysis were of dimension 15.5 mm×9.6 mm×2.3 mm, while those for electrochemical measurements were cylindrical in shape with an exposed surface area of 2.0 cm^2 leaving the remaining part embedded in epoxy resin. Prior to each experiment, the specimen was wet ground with abrasive paper of increasing fineness up to 800 grits, rinsed with distilled water, cleaned with ethanol and dried in air. The corrosive solution was 1.0 M HCl which was prepared from 36.5% HCl (analytical grade, supplied by Chongqing Chuandong Chemical Group Co., Ltd.) and distilled water. The inhibitor of 1-butyl-3-methyl-1H-benzimidazolium iodide was supplied by Shanghai Chengjie Chemical Co., Ltd., its purity was 99%, and no further purification before use.

Table 1. Chemical composition of 2205 duplex stainless steel.

Element	C	Cr	Ni	Mo	Mn	S	Fe
wt%	< 0.03	22.00	5.00	3.30	2.00	0.03	Bal.

2.2 Electrochemical measurements

Electrochemical measurements were performed using the CHI660E electrochemical work station (Supplied by Shanghai Chenhua Instrument Co., Ltd.) with a conventional three-electrode cell, which contained a platinum grid, a saturated calomel electrode (SCE) and 2205 DSS working electrode. All potential data reported were referred to SCE reference electrode. For stability of the sample surface, open circuit potential (OCP) was first conducted for 60 minutes. The EIS measurements were performed at OCP with a sinusoidal potential perturbation of 5 mV in a frequency range from 100 kHz to 0.01 Hz.

Potentiodynamic polarization measurements were conducted in the potential range of -0.25 V to + 0.50 V versus OCP at a scan rate of 1.0 mV/s.

2.3 Surface analysis

Test coupons were immersed in the solution without and with 5.0 mM BMBM at 303 K for 168 hours. After the test duration, the samples were retrieved, gently rinsed with distilled water, dipped in acetone and dried in air. The surface morphology of the sample surface was examined with VEGA 3SBU scanning election microscope (SEM) (Supplied by Bruker Analytical Instruments).

3. RESULTS AND DISCUSSION
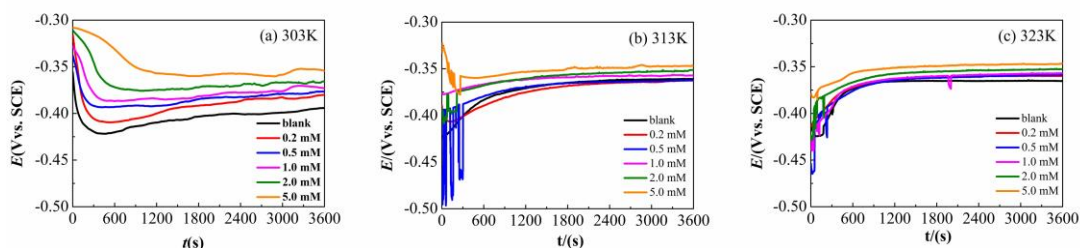
3.1 Open circuit potential

Figure 2. Open circuit potential versus time curve of 2205 duplex stainless steel in 1.0 M HCl containing different concentrations of BMBM at different temperatures.

Figure 2 shows the OCP versus time curves of 2205 DSS in 1.0 M HCl with different concentrations of BMBM at 303 K, 313 K, and 323 K. It can be seen from the Figure 2 that the OCPs were progressively shifted to the positive directions with the addition of BMBM, and with increasing concentration of the inhibitor, the value of the OCPs further increased, indicating that the inhibitor was adsorbed on the surface of 2205 DSS and thus, inhibiting its corrosion in hydrochloric acid solution. It can also be seen from Figure 2 that the OCP of 2205 DSS electrode in the test solution begins to stabilize at 1800 s.

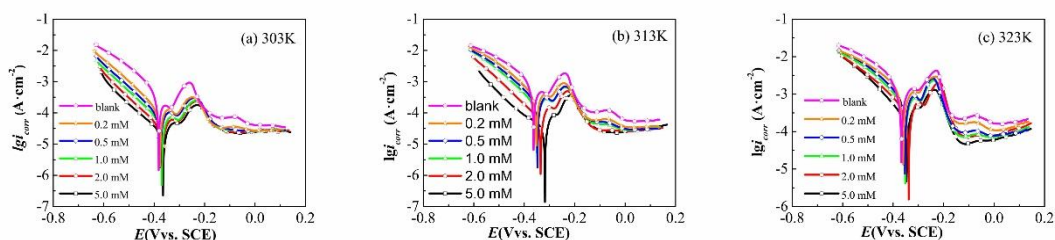### 3.2 Potentiodynamic polarization curves

Figure 3. Potentiodynamic polarization curves of 2205 DSS in 1.0 M HCl containing different concentrations of BMBM at different temperatures.

Figure 3 gives the potentiodynamic polarization curves of 2205 DSS in the absence and presence of different concentrations of BMBM at 303 K, 313 K, and 323 K. The potentiodynamic polarization parameters such as the corrosion potential (E_{corr}), cathodic Tafel slopes (β_c), and corrosion current density (i_{corr}) which were extrapolated from the fitting of the potentiodynamic polarization curves are listed in Table 2.

For all temperatures, the forms of these curves are very similar in both the cathodic and anodic branches, indicating that the mechanisms of 2205 DSS electrochemical reactions remained invariant without and with the inhibitor [24-26]. It can be seen that with the addition of BMBM, the corrosion potential increased but corrosion current density reduced, this may be due to the adsorption of the inhibitor on the electrode surface. Besides, the current density on the anodic polarization curve showed a two-fold reduction process, which means that there are two passivation intervals in the 2205 DSS in 1.0 M HCl. This may be attributed to passivation or deposition of corrosion products obtained from the different phases (austenite and ferrite) in 2205 DSS [27].

Figure 3 also shows that the addition of BMBM in the studied temperature range makes the anode branch and cathode branch of the polarization curve move towards the direction of low current density, which shows that BMBM can inhibit the cathode and anode reactions of 2205 DSS electrode in HCl, and the inhibition increases in turn with the increase of inhibitor concentration. Although the addition of BMBM caused the corrosion potentials to shift positively, but the shifts were all less than 85 mV. Therefore, the BMBM behaved as a mixed-type inhibitor [28-33]. Values for corrosion inhibition efficiency ($\eta\%$) presented in Table 2 are obtained from equation (1) as shown:

$$\eta(\%) = (1 - \frac{i_{corr}}{i_0}) \times 100 \quad \dots\dots\dots\dots\dots\dots\dots\dots\dots\dots\dots\dots\dots\dots\dots\dots\dots\dots\dots\dots\dots\dots\dots\dots$$

(1)

Where i_0 and i_{corr} are corrosion current densities in the absence and presence of the inhibitor, respectively.

Table 2. Potentiodynamic polarization parameters of 2205 DSS in 1.0 M HCl containing different concentrations of BMBM at 303 K, 313 K, and 323 K.

T (K)	C (mM)	$-E_{corr}$ (mV vs SCE)	$-\beta_c$	i_{corr} (μA/cm^2)	η (%)
	blank	382	143	456	-
	0.2	377	128	113	75.3
303	0.5	376	130	77	83.1
	1.0	370	132	51	88.7
	2.0	369	137	33	92.7
	5.0	365	147	23	95.1
	blank	363	174	940	-
	0.2	351	139	339	63.9
313	0.5	348	136	230	75.5
	1.0	350	132	178	81.1
	2.0	335	130	60	93.7
	5.0	318	171	29	96.9
	blank	367	192	1862	-
323	0.2	360	194	1253	32.7
	0.5	353	159	710	61.9

1.0	352	155	562	69.8
2.0	338	151	317	83.0
5.0	347	135	222	88.1

As observed from Table 2, the $\eta\%$ values show that the corrosion inhibition efficiency increased with increasing inhibitor concentration, with the highest inhibition efficiency being 96.9% for 5.0 mM/L at 313 K. The increase in $\eta\%$ with inhibitor concentration is possibly the result of the corresponding increase in the number of absorbed molecules on the surface of the specimen, thereby blocking the active sites for acid attack.

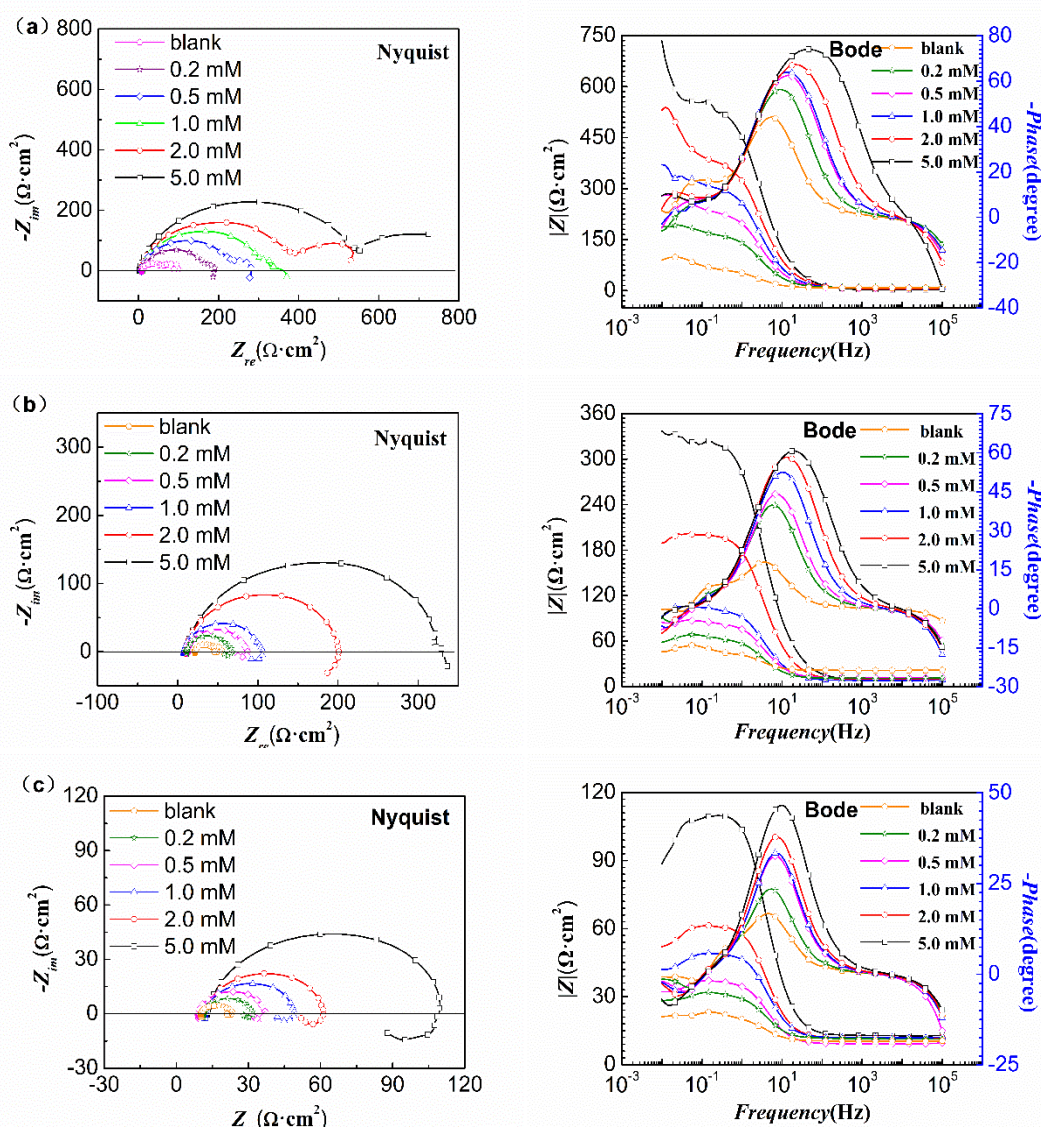### 3.3 Electrochemical impedance spectroscopy measurements

Figure 4. Nyquist and Bode diagrams of 2205 DSS in 1.0 M HCl containing different concentrations of BMBM at different temperatures. (a) 303 K (b) 313 K (c) 323 K.

Figure 4 shows the EIS spectra of 2205 DSS in 1.0 M HCl without and with different concentrations of BMBM at different temperatures. As observed in the polarization curves, the shapes of the spectra are very similar for all temperatures and concentrations, indicating that no change occurred in the corrosion mechanism of 2205 DSS in 1.0 M HCl with the addition of the inhibitor. Additionally, the diameter of the Nyquist plots increased with increasing concentration of BMBM. The middle and high frequency regions of the Nyquist and Bode plots of 2205 DSS in the test solutions at different temperatures are identical, showing a characteristic one time constant. However, small inductive loops are observed at low frequency regions in Figure 4 (b) and (c), which can be attributed to the effect of temperature on the corrosion behavior of 2205 DSS and the and the adsorption behavior of corrosion inhibitor.

To obtain the EIS parameters, the electrical equivalent circuits [34, 35] shown in Figure 5 are used to simulate the obtained EIS data of the middle and high frequency regions by ZSimpWin software. The impedance parameters obtained from the fitting are shown in Table 3. R_s is the solution resistance, CPE_{dl} is the metal interface capacitance, Y_0 is the CPE constant, n is the phase shift which amounts to the degree of surface inhomogeneity, and R_{ct} is the charge transfer resistance of the metal-electrolyte interface. The R_{ct} values are used to calculate the inhibition efficiency ($\eta\%$) according to the following equation:

$$\eta(\%) = (1 - \frac{R_{ct}^0}{R_{ct}}) \times 100 \quad\dots\dots\dots\dots\dots\dots\dots\dots\dots\dots\dots\dots\dots\dots\dots\dots\dots\dots\dots\dots\dots\dots\dots(2)$$

Where R^0_{ct} and R_{ct} are the charge transfer resistances in the absence and presence of BMBM, respectively.
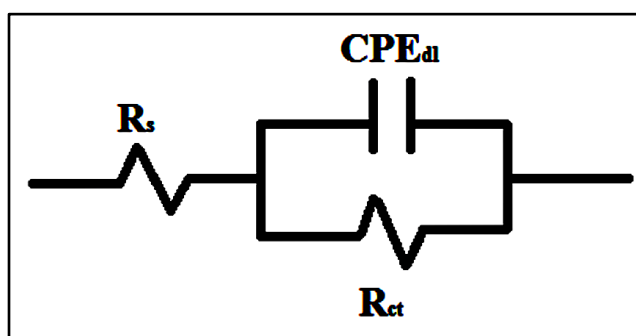

Figure 5. Equivalent circuit for the fitting of EIS data of the middle and high frequency regions of 2205 DSS in 1.0 M HCl.

Table 3. Impedance parameters of 2205 DSS in 1.0 M HCl containing different concentrations of BMBM at 303 K, 313 K, and 323 K.

T (K)	C (mM)	R_s ($\Omega\cdot$cm^2)	Y_0 (μF/cm^2)	n	R_{ct} ($\Omega\cdot$cm^2)	η (%)
	blank	8.31	1968	0.9191	91.3	-
303	0.2	9.83	616	0.9275	181.4	49.7
	0.5	7.63	433	0.9190	222.7	59.0
	1.0	8.73	334	0.9204	330.4	72.4

	2.0	6.21	254	0.9049	375.6	75.7
	5.0	2.36	172	0.9121	514.7	82.3
	blank	11.37	3112	0.9363	33.3	-
	0.2	10.86	1664	0.9100	55.0	39.5
313	0.5	11.34	1083	0.9207	74.0	55.0
	1.0	8.06	833	0.9201	95.6	65.2
	2.0	9.51	428	0.9146	192.6	82.7
	5.0	9.09	284	0.8797	319.0	89.6
	blank	10.32	8333	0.8344	12.7	-
	0.2	11.52	3496	0.9063	20.1	36.9
323	0.5	9.22	2170	0.9281	27.7	54.3
	1.0	11.89	1531	0.9331	37.4	66.1
	2.0	11.84	1254	0.9315	49.7	74.5
	5.0	12.89	665	0.9243	99.1	87.2

From the data in Table 3, as the concentration of BMBM increased for a given temperature, the values of R_{ct} increased and Y_0 decreased. The increase in charge transfer resistance may be due to the increase in the adsorption of the inhibitor films on the surface of 2205 DSS, resulting in better inhibition efficiency [21]. Capacitance reduction may be the result of either a decrease in the local dielectric constant or an increase in thickness of the electric double layer, or a combination of both scenarios [36, 37]. These indicate the adsorption of the inhibitor molecules at the metal/solution interface. As the concentration increased, the inhibition efficiency increased, while as the temperature increased, the inhibition efficiency decreased. The corrosion inhibition efficiency value calculated by EIS measurements is basically consistent with the results obtained from the polarization measurements.
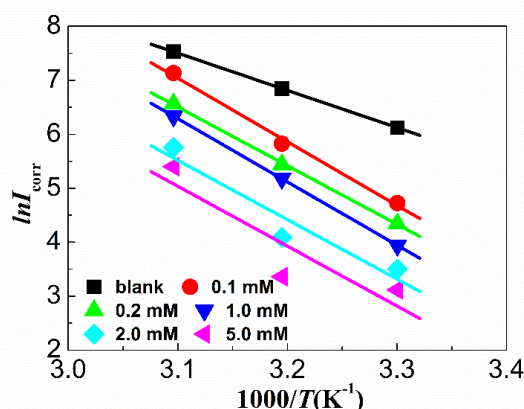
3.4 Effect of temperature

Figure 6. Arrhenius plots of 2205 DSS in 1.0 M HCl without and with different concentrations of BMBM

Data from Table 2, corresponding to the extrapolated parameters from the potentiodynamic polarization curves, are analyzed to understand the effect of temperature on the corrosion inhibition of 2205 DSS in 1.0 M HCl without and with BMBM. It was observed that with increasing temperature, the

value of the corrosion current density increased, and the values of η were decreasing. This may have resulted from a reduced adsorption rate of BMBM on the metal surface, which led to the exposure of active sites to the aggressive solution and consequently, an acceleration of the corrosion process. However, at the concentrations of 2.0 and 5.0 mM, the values of η increased as the temperature increased from 303 K to 313 K. This may have been due to the change in the nature of the adsorption mode [14].

In order to calculate the activation parameters for the corrosion process, the extrapolated data in Table 2 were fitted to the Arrhenius equation (equation 3) and the results are presented in Figure 6.

$$ln\,i_{corr} = lnA - \frac{E_a}{RT} \dots\dots\dots\dots\dots\dots\dots\dots\dots\dots\dots\dots\dots\dots\dots\dots\dots\dots\dots\dots\dots\dots\dots\dots..(3)$$

Where E_a is the apparent activation corrosion energy, T is the absolute temperature, A is the Arrhenius pre-exponential constant and R is the universal gas constant. Kinetic parameters for the adsorption of inhibitors can provide valuable information about the mechanism of corrosion inhibition [21, 38]. The calculated values of the apparent activation corrosion energy in the absence and presence of BMBM are listed in Table 4.

Table 4. Kinetic parameters of BMBM adsorption on 2205 DSS immersed in 1.0 M HCl.

C (mM)	R	A	E_a (kJ/mol)
Blank	0.9999	3.36×10^{12}	57
0.2	0.9977	8.01×10^{18}	98
0.5	0.9996	2.76×10^{17}	90
1.0	0.9999	3.11×10^{18}	97
2.0	0.9586	1.57×10^{17}	91
5.0	0.9027	1.32×10^{17}	92

Usually, increase of E_a in the presence of inhibitor indicates that a physical (electrostatic) adsorption occurred [39], whereas the decline of E_a with the addition of inhibitor suggests that there is a strong chemisorption between the inhibitor molecules and the metal surfaces [40, 41]. According to the Table 4, the addition of BMBM led to an obvious increase in E_a to values greater than that of the uninhibited solution, which means that the function of BMBM is mainly physical adsorption. The value of A also increased significantly, indicating that the degree of corrosion of the 2205 DSS was not only affected by the activation energy, but also by the pre-exponential factor.

3.5 Adsorption isotherm

In order to understand the mechanism between BMBM and the metallic surface, the data are fitted into different adsorption isotherm models such as Langmuir, Temkin, Frumkin, etc. The Langmuir adsorption isotherm model was found to be the most suitable for the generated data [42-44]. The general equation of this isotherm is as shown:

$$\frac{C}{\theta} = \frac{1}{K_{ads}} + C \dots\dots\dots\dots\dots\dots\dots\dots\dots\dots\dots..\dots\dots\dots\dots\dots\dots\dots\dots\dots\dots\dots..(4)$$

Where θ is the surface coverage of the metal surface, K_{ads} the adsorption–desorption equilibrium constant, C the inhibitor concentration. The equation can be used to calculate the K_{ads} values of the

corrosion reaction without and with inhibitor. The Langmuir adsorption plots obtained from the data of the polarization curves and EIS spectra are presented in Figure 7, and the values of K_{ads} are listed in Table 5. Figure 7 shows a significant linear relationship between the experimental data points, and the linear fitting correlation coefficient (R) is approximately one, which indicates that the adsorption of inhibitor on the surface of 2205 DSS conforms to the Langmuir adsorption isotherm equation.
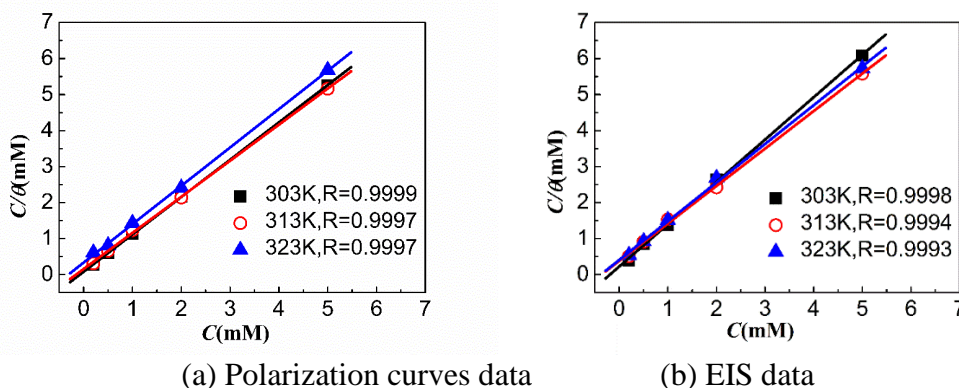

(a) Polarization curves data   (b) EIS data

Figure 7. Langmuir adsorption plots obtained from polarization and EIS measurements for 2205 DSS in 1.0 M HCl at different temperatures.(a) polarization curves data (b) EIS data

Table 5. Thermodynamics parameters of BMBM adsorption on 2205 DSS immersed in 1.0 M HCl at different temperatures.

T (K)	Polarization curve				EIS			
	K_{ads} (L/mol)	ΔG_{ads} (kJ/mol)	$\Delta_r H_{ads}$ (kJ/mol)	$\Delta_r S_{ads}$ (kJ/mol)	K_{ads} (L/mol)	ΔG_{ads} (kJ/mol)	$\Delta_r H_{ads}$ (kJ/mol)	$\Delta_r S_{ads}$ (kJ/mol)
303	12571	-34			4463	-31		
313	6341	-33	-57	-109	2642	-31	-25	-12
323	2991	-32			2465	-32		

The values of the entropy of activation ($\Delta_r S_{ads}$), the enthalpy of activation ($\Delta_r H_{ads}$) and the free energy of adsorption (ΔG_{ads}) are calculated according to Van 't Hoff equation as shown [42-44]:

$$K_{ads} = \frac{1}{55.5} \exp\left(-\frac{\Delta G_{ads}}{RT}\right) \quad\text{...(5)}$$

$$ln K^{\Phi} = -\frac{\Delta_r H_{ads}}{RT} + \frac{\Delta_r S_{ads}}{R} \quad\text{..(6)}$$

Where R is the universal gas constant, T is the absolute temperature. The fitting plots of K_{ads} on the 2205 DSS surface by the Van 't Hoff equation are illustrated in Figure 8. While the values of the $\Delta_r S_{ads}$ and the $\Delta_r H_{ads}$ are also presented in Table 5.
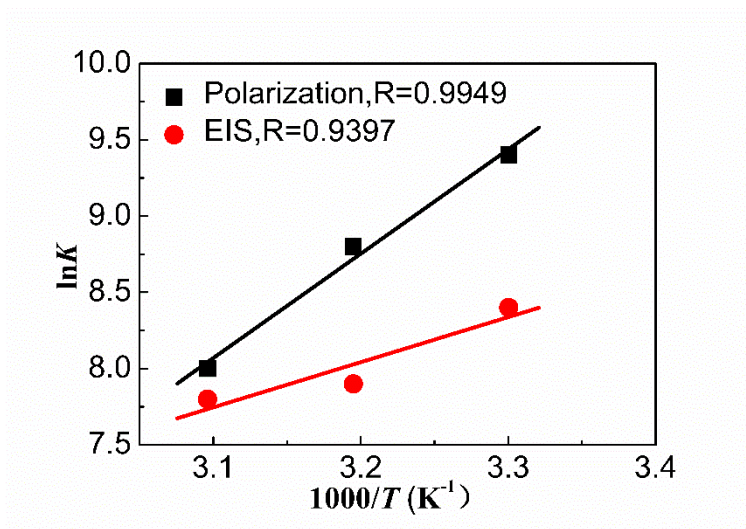
Figure 8. Fitting diagram of K_{ads} versus Van't Hoff equation for the adsorption of BMBM on the surface of 2205 DSS.

With increase in temperature, the adsorption equilibrium constant (K_{ads}) of the corrosion inhibitor gradually decreased, indicating that the adsorption capacity on the surface of 2205 DSS gradually decreased, which corresponds to the decrease in corrosion inhibition efficiency with increasing temperature. The values of ΔG_{ads} at different temperatures ranges from -35 kJ/mol to -30 kJ/mol, which means that the interaction between the inhibitor and the surface of 2205 DSS involved both physisorption and chemisorption [45, 46], but with the values around -30 kJ/mol, physisorption was probably the dominant interaction. The negative value of $\Delta_r H_{ads}$ suggests that the adsorption reaction was an exothermic process. Additionally, the values of $\Delta_r S_{ads}$ is also less than zero, indicating that stable adsorption film formed on the surface of 2205 DSS, thereby reducing the freedom of transfer of molecules.
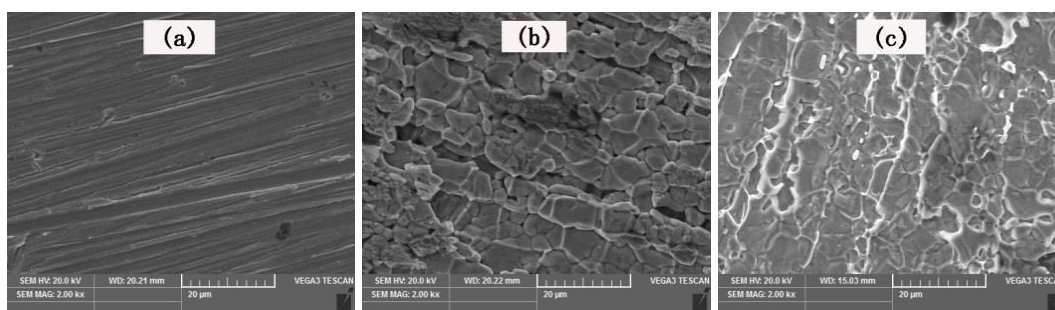
3.6 Surface analysis

Figure 9. SEM micrographs of 2205 DSS (a) unexposed, (b) exposed to 1.0 M HCl and (c) exposed to 1.0 M HCl solution containing 5.0 mM BMBM.

Figure 9 shows the SEM micrographs of 2205 DSS samples before and after immersion in 1.0 M HCl solution without and with 5.0 mM BMBM for 168 hours at 303 K. It can be clearly observed

from the Figure that the surface of the sample immersed in the solution without BMBM was greatly corroded. While the extent of damage was much reduced for the sample exposed to the acid solution containing BMBM. This indicates that BMBM can effectively inhibit the corrosion reaction on the surface of 2205 DSS exposed to an acid environment containing the ionic liquid.

4. CONCLUSIONS

(1) BMBM acted as a good mixed-type inhibitor for corrosion of 2205 DSS in 1.0 M HCl solution, and its inhibition efficiency increased with increasing concentration of the inhibitor, and the highest inhibition efficiency reached 96.9%.

(2) The inhibition efficiency reduced as the temperature increased, confirming the adsorption of BMBM on 2205 DSS surface. The adsorption process is spontaneous and follows the Langmuir adsorption isotherm.

References

1. Z. Zhang, Z. Hui, H. Zhang, J. Hu and J. Jin, *Corros. Sci.,* 121 (2017) 22.
2. J. Lv, W. Guo and T. Liang, *J. Alloys Compd.,* 686 (2016) 176.
3. M. Naghizadeh and M.H. Moayed, *Corros. Sci.,* 94 (2015) 179.
4. M. Zakeri and M.H. Moayed, *Corros. Sci.,* 85 (2014) 222.
5. M. Hoseinpoor, M. Momeni, M.H. Moayed and A. Davoodi, *Corros. Sci.,* 80 (2014) 197.
6. C. Örnek and D.L. Engelberg, *Mater. Sci. Eng., A.* 666 (2016) 269.
7. W. Yi, X. Cheng and X. Li, *Electrochem. Commun.,* 57 (2015) 56.
8. J.S. Lee, K. Fushimi, T. Nakanishi, Y. Hasegawa and Y.S. Park, *Corros. Sci.,* 89 (2014) 111.
9. J. C. D. Lacerda, L. C. Cândido and L.B. Godefroid, *Mater. Sci. Eng., A.* 648 (2015) 428.
10. N. Dai, J. Wu, L.-C. Zhang, L. Yin, Y. Yang, Y. Jiang and J. Li, *Constr. Build. Mater.,* 202 (2019) 877.
11. P.O. Malta, F.L. Dias, A.C.M. Souza and D.B. Santos, *Mater. Charact.,* 142 (2018) 406.
12. A. Ehsani, M.G. Mahjani, M. Hosseini, R. Safari, R. Moshrefi and H.M. Shiri, *J. Colloid Interface Sci.,* 490 (2017) 444.
13. M. Mehdipour, B. Ramezanzadeh and S.Y. Arman, *J. Ind. Eng. Chem*., 21 (2015) 318.
14. F. Kurniawan and K.A. Madurani, *Prog. Org. Coat.,* 88 (2015) 256.
15. L. Aparecida Corrêa Matos, M.C Taborda, G.J.T. Alves, M.T. Cunha, E.P. Banczek, M.F. Oliveira, E.D. Elia and P.R.P. Rodrigues, *Int. J. Electrochem. Sci*., 13(2018) 1577.
16. N. Soltani, N. Tavakkoli, M.K. Kashani, A. Mosavizadeh, E.E. Oguzie and M.R. Jalali, *J. Ind. Eng. Chem.,* 20 (2014) 3217.
17. E. Kowsari, S.Y. Arman, M.H. Shahini, H. Zandi, A. Ehsani, R. Naderi, A. PourghasemiHanza and

M. Mehdipour, *Corros. Sci.,* 112 (2016) 73.

18. J.H. Ha, J.H. Cho, J.H. Kim, B.W. Cho and S.H. Oh, *J. Power Sources.,* 355 (2017) 90.
19. A.L. Chong, M. Forsyth and D.R. MacFarlane, *Electrochim. Acta.,* 159 (2015) 219.
20. S.K Shetty and A.N. Shetty, *J. Mol. Liq.,* 225 (2017) 426.
21. X.W. Zheng, S.T. Zhang, W.P. Li, M. Gong and L.L. Yin, *Corros. Sci.,* 95 (2015) 168.
22. P. Kannan, J. Karthikeyan, P. Murugan, T.S. Rao and N. Rajendran, *J. Mol. Liq.,* 221 (2016) 368.
23. C. Liu, M. Gong, X.W. Zheng, *Int. J. Electrochem. Sci*., 13 (2018) 7432.
24. O. Kaczerewska, R. Leiva-Garcia, R. Akid and B. Brycki, *J. Mol. Liq.,* 247 (2017) 6.
25. O. Kaczerewska, R. Leiva-Garcia, R. Akid, B. Brycki, I. Kowalczyk and T. Pospieszny, *J. Mol. Liq.,* 249 (2018) 1113.
26. N.D. Nam, P.V. Hien, N.T. Hoai and V.T.H. Thu, *J. Taiwan. Inst. Chem. Eng.,* 91 (2018) 556.
27. Y. Wang, X.Q. Cheng and X.G. Li, *Electrochem. Commun.,* 57 (2015) 56.
28. M. Shabani-Nooshabadi and M.S. Ghandchi, *J. Ind. Eng. Chem.,* 31 (2015) 231.
29. M. Mehdipour, B. Ramezanzadeh and S.Y. Arman, *J. Ind. Eng. Chem.,* 21 (2015) 318.
30. A. Ehsani, M.G. Mahjani, M. Hosseini, R. Safari, R. Moshrefi and H.M. Shiri, *J. Colloid Interface Sci.,* 490 (2017) 444.
31. R.T. Loto, C.A. Loto, O. Joseph and G. Olanrewaju, *Results Phys.,* 6 (2016) 305.
32. P. Thanapackiam, S. Rameshkumar, S.S. Subramanian and K. Mallaiya, *Mater. Chem. Phys.,* 174 (2016) 129.
33. K.F. Khaled and A. El-Maghraby, *Arab. J. Chem.,* 7 (2014) 319.
34. S.A. Umoren, A.A. Alahmary, Z.M. Gasem and M.M. Solomon, *Int. J. Biol. Macromol.,* 117 (2018) 1017.
35. R.S. Erami, M. Amirnasr, S. Meghdadi, M. Talebian, H. Farrokhpour and K. Raeissi, *Corros. Sci.,* 151 (2019) 190.
36. T. He, W. Emori, R.-H. Zhang, P.C. Okafor, M. Yang, C.R. Cheng, *Bioelectrochem*., 130 (2019) 107332.
37. G. Karthik and M. Sundaravadivelu, *Egypt. J. Pet.,* 25 (2016) 183.
38. R.M. Hassan, S.M. Ibrahim, H.D. Takagi and S.A. Sayed, *Carbohydr. Polym.,* 192 (2018) 356.
39. H. Hamani, T. Douadi, D. Daoud, M. Al-Noaimi, R.A. Rikkouh and S. Chafaa, *J. Electroanal. Chem.,* 801 (2017) 425.
40. I. Aiad, S.M. Shaban, A.H. Elged and O.H. Aljoboury, *Egypt. J. Pet.,* 27 (2018) 877.
41. A.A. Khadom, A.N. Abd and N.A. Ahmed, *S. Afr. J. Chem.,* 25 (2018) 13.
42. H. Lgaz, M. Chung, R. Salghi, I.H. Ali, A. Chaouiki, Y.E. Aoufir and M.I. Khan, *Appl. Surf. Sci.,* 463 (2019) 647.
43. P. Singh and M.A. Quraishi, *Measurement.,* 86 (2016) 114.
44. A.S. Fouda, S.M. Rashwan, S.M. Shaban, H.E. Ibrahim and M.F. Elbhrawy, *Egypt. J. Pet.,* 27 (2018) 295.
45. A. Hamdy and N.S. El-Gendy, *Egypt. J. Pet.,* 22 (2013) 17.
46. A.F.S.A Rahiman and S. Sethumanickam, *Arab J. Chem.,* 10 (2017) S3358.